Available online at www.sciencedirect.com
SCIENCE DIRECT®
Journal of Crystal Growth 276 (2005) 1–6
JOURNAL OF CRYSTAL GROWTH
www.elsevier.com/locate/jcrysgro

Simultaneous growth of Si_3N_4 nanobelts and nanodendrites by catalyst-assisted crystallization of amorphous SiCN

Weiyou Yang[a], Zhipeng Xie[a,*], Hezhuo Miao[a], Ligong Zhang[b], Linan An[b,c]

[a]*State Key Lab of New Ceramics and Fine Processing, Tsinghua University, Beijing 100084, China*
[b]*Laboratory of Excited State Process, Changchun Institute of Optics, Fine Mechanics and Physics, Chinese Academy of Sciences, Changchun, China*
[c]*Advanced Materials Processing and Analysis Center, University of Central Florida, Orlando, FL 32816, USA*

Received 4 August 2004; accepted 23 September 2004
Communicated by A.Y. Cho
Available online 28 January 2005

Abstract

Si_3N_4 nanobelts and nanodendrites were simultaneously synthesized via a novel catalyst-assisted crystallization of polymer-derived amorphous silicon carbonitride. The single crystal nanobelts, with a uniform cross-section of 20–30 nm in thickness and 100–300 nm in width, can grow up to a few millimeters in length. The nanodendrites consist of a plate-like stem and nanobelts branches of 10–20 nm thick and 50–150 nm wide. The branches that are up to 50 μm in length grew only along the middle line of the stem with regular spacing. A growth for both nanobelts and nanodendrites is attributed to a solid–liquid–gas–solid process.

Keywords: A2. Catalyst-assisted crystallization; B1. Nanobelts; B1. Nanodendrites

1. Introduction

Silicon nitride (Si_3N_4) has attracted great attention in the last decades for its excellent thermal and mechanical properties for structural applications at both ambient and elevated temperatures [1,2]. Similar to III-N compounds such as GaN and AlN, Si_3N_4 is also an excellent host material in terms of high dopant concentration, mechanical and thermal properties and chemical stabilities. It has been demonstrated that by introducing mid-gap levels into the wide band gap of ~5.3 eV in nondoped Si_3N_4, the emission of green to ultraviolet light can be achieved [3–6]. The synthesis of Si_3N_4 nanomaterials is of particular interest since they could be promising candidates for fabricating nanocomposites and electronic/optic nanodevices that can be operated at extreme conditions such as

*Corresponding author.
E-mail addresses: zpx@mails.tsinghua.edu.cn (Z. Xie), lan@mail.ucf.edu (L. An).

0022-0248/$ - see front matter © 2004 Published by Elsevier B.V.
doi:10.1016/j.jcrysgro.2004.09.099

high temperatures, corrosive environments, high power and radiation environments. The synthesis of Si_3N_4 nanowires has been reported [7–10]. It was demonstrated that Si_3N_4 nanowires possess much higher bending strength than the bulk [7]. Recently, Yin et al. reported the synthesis of α-Si_3N_4 nanobelts via a vapor–solid thermal reaction between ammonia and silicon monoxide (SiO) and observed intense visible photoluminescence over a broad spectrum ranging from 420 to 750 nm [11].

In this communication, we report the simultaneous growth of α-Si_3N_4 nanobelts and nanodendrites via a novel catalyst-assisted crystallization of polymer-derived amorphous silicon carbonitride (SiCN). A similar technique has been used to synthesize SiC nanorods [12]. While nanodendrite-like structures have been synthesized in various materials [13–20], to the best of our knowledge, this is the first time that Si_3N_4 dendrites have been reported. Furthermore, the trunks and branches of nanodendrites reported previously are either nanowires [13,15], nanotubes [14] or nanoneedles [16,17], both trunks and branches of the Si_3N_4 nanodendrites reported here possess belt-like structures. The morphologies and structures of the nanobelts and nanodendrites were fully characterized. A growth mechanism is discussed. It is anticipated that the novel structures will have some unique applications in fabricating three-dimensional nanocomposites and nanodevices.

2. Experimental procedure

Amorphous SiCN was synthesized by thermal decomposition of a commercially available polyureasilazane (Ceraset^{TM}, Kion Corporation, US). The as-received Ceraset, which is a liquid at room temperature, was first solidified by heat-treatment at 260 °C for 0.5 h in N_2 [21]. The obtained solid was then crushed into fine powder by high-energy ball milling for 24 h with an addition of 3 wt% Al fine powders (98% purity, containing Fe, Ni and Cr impurities, Beijing Bei Hua Fine Chemicals Company Ltd. Beijing, China). The powder mixture was then placed in a high-purity alumina crucible and pyrolysized in a conventional furnace with graphite resistance under flowing ultra-high purity nitrogen of 0.1 MPa. The powder mixture was heated to 1300 °C at 10 °C/min and held there for 4 h followed by furnace-cool. The experiments were also performed on the samples without Al additives for comparison.

The morphology, structure and composition of the pyrolysis products were characterized using field emission scanning electron microscopy (SEM, JSM-6301, JEOL, Japan), X-ray diffraction (XRD, Automated D/Max-RB, Rigaku, Japan) with CuKα radiation ($\lambda = 1.54178$ Å), and high-resolution transmission electron microscope (HRTEM, JEOL-2010F, Japan) equipped with energy dispersive X-ray spectrum (EDS).

3. Results and discussion

The morphologies of the pyrolyzed products were first examined using SEM. The most typical structure observed is Si_3N_4 nanobelts (Fig. 1a). By measuring over 100 belts, it was found that the thickness of the nanobelts ranges from 20 to 30 nm, the width from 100 to 300 nm, and the length from a few hundred micrometers to several millimeters. Within each individual belt, the thickness and width are uniform along its entire length. The presence of highly curved belts suggests that they possess extensive flexibility. A closer examination of the belts at high magnification (Fig. 1b) reveals that the surfaces of the belts are smooth and clear. SEM observation (Fig. 1b) also discovered that there are no liquid droplets at the tips of the belts, which were typically observed in vapor–liquid–solid (VLS) growth in the presence of catalysts [22], indicating the reported nanobelts grew by fundamentally different mechanisms.

Beside the nanobelts, the growth of nanodendrites has also been observed. Fig. 2 shows the SEM images of the nanodendrites grew at different stages. It can be seen that the dendrite structures typically consist of a plate-like stem and very long belt-like branches. The thickness and width of the stem are about 200 and 500 nm, respectively; the length can be up to hundreds of micrometers. The branches possess a nanobelt-like cross-section with a uniform thickness and width along the

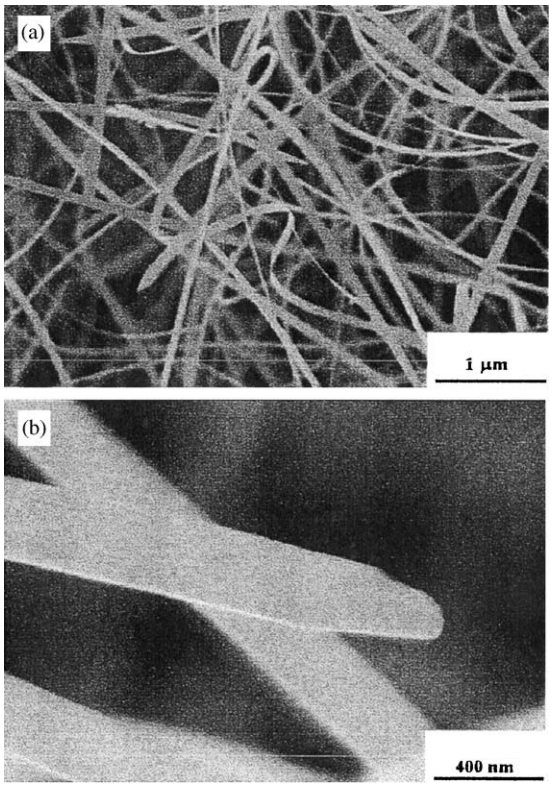

Fig. 1. SEM images showing (a) the morphology of the nanobelts at low magnification and (b) rectangular cross-section with clean surfaces.

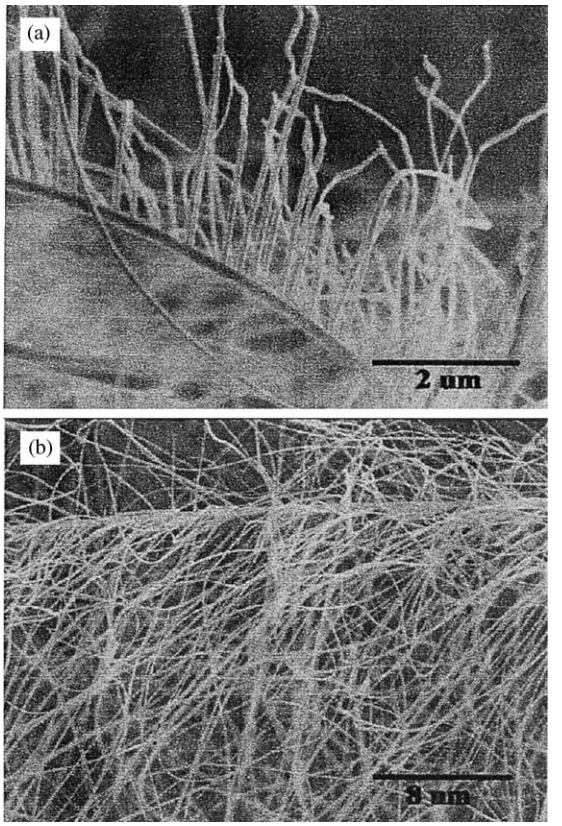

Fig. 2. SEM images showing (a) the growth of nanodendrites at earlier stages and (b) fully grown nanodendrites.

growth direction, which is fundamentally different from those previously observed in other material systems where the branches possess the morphology of either nanowires, nanotubes or nanoneedles [13–17]. The thickness and width of the branches were about 10–20 nm and 100–200 nm, respectively; and the length can be up to more than 50 μm. The SEM observation at different growth stages also revealed that the density and cross-section geometry of the branches remain the same, but the length increases with time, suggesting that the nanobelt branches are grown from the stem instead of joining between the grown belts and the stem.

The crystalline structure of the pyrolyzed products was first examined using XRD (Fig. 3). It can be seen that pyrolyzed products contain α-Si_3N_4 phase only. The broad hump at lower angle regions suggests that the unconverted powder remains amorphous.

Further characterization of the morphologies and structure of the nanobelts was carried out using TEM and HRTEM. Figs. 4a and b show typical TEM images of straight and curved Si_3N_4 nanobelts, respectively. The images further reveal that the nanobelts are very thin and transparent to electrons. The ripple-like contrast is due to the residual strain. EDS analysis shows that the nanobelts contain Si and N only with atomic ratio of the two close to that in Si_3N_4. Figs. 4c and d are HRTEM lattice images with the corresponding SAED. The images show that the nanobelts possess perfect crystal structure with few defects such as dislocations and stacking faults. The HRTEM analysis on more than 20 belts revealed that there are only two distinguished lattice fringe

patterns. The lattice fringe spacings of 0.56 and 0.67 nm in Fig. 4c agree well with (0 0 1) and (0 1 0) planes of hexagonal α-Si_3N_4 with $a = 0.77541$ nm and $c = 0.56217$ nm (JCPDS Card no. 41-0360); and the lattice fringe spacing of 0.67 nm in Fig. 4d corresponds to (1 0 0) plane. The HRTEM and SAED analysis suggest that the belts grow along two directions: [0 1 1] (Fig. 4c) and [1 0 0] (Fig. 4d). Within each belt, HRTEM and SAED patterns are identical throughout the entire belt, indicating that the belts are single crystal.

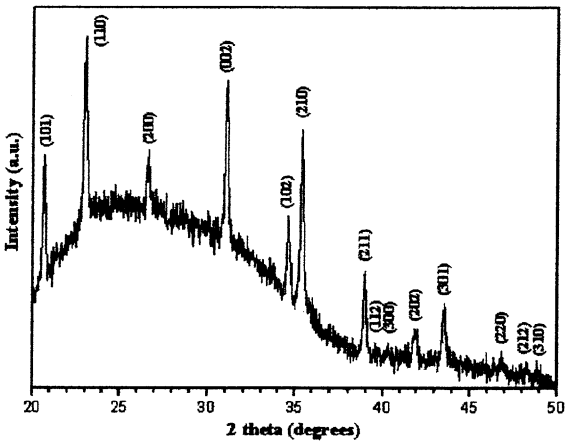

Fig. 3. XRD pattern of as-synthesized products indicated that α-Si_3N_4 is only crystalline phase.

The morphologies and structure of the nanodendrites were also analyzed using TEM and HRTEM. TEM observations (Fig. 5a) on the nanodendrites confirm that the stem possesses plate-like shape and the branches are nanobelts with a uniform thickness and width along the growth direction. Fig. 5a also reveals that there is a dark spot between the end of branch and the stem. EDS analysis on these dark spots (inset in Fig. 5a) reveals that they consist of Fe, Ni, Cr and Si (Cu signal results from sample holder). The Fe, Ni and Cr are from the impurity of the catalyst (see experimental procedure); but it is surprising that

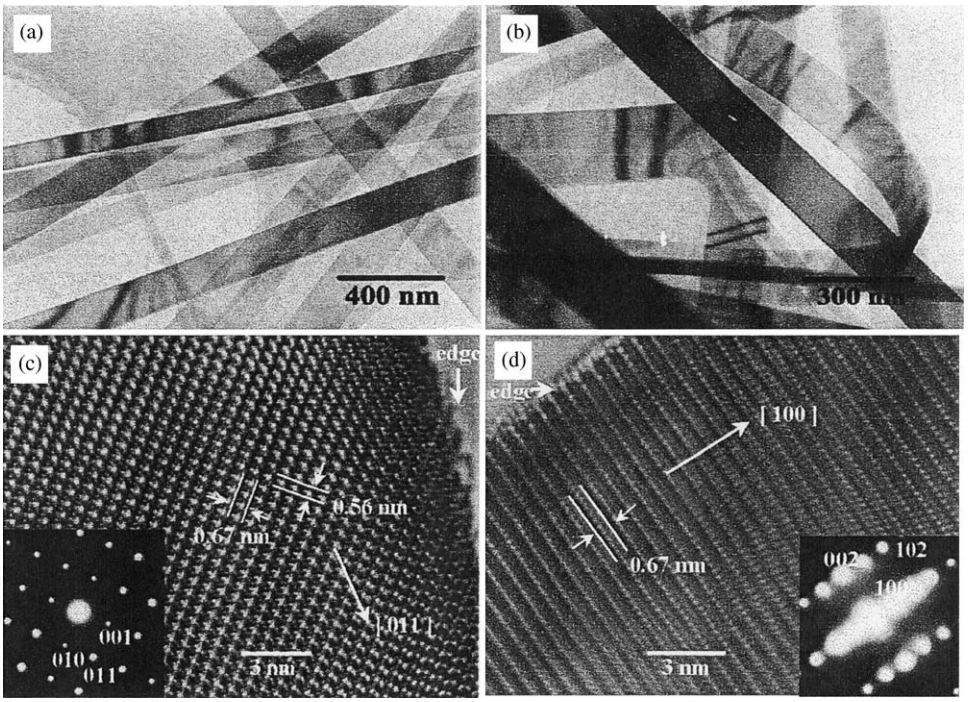

Fig. 4. (a) and (b) typical TEM images show both straight and curved Si_3N_4 nanobelts; (c) HRTEM image and corresponding SAED (inset) pattern of nanobelts that grew along [0 1 1] direction; (d) HRTEM image and corresponding SAED (inset) pattern of nanobelts that grew along [1 0 0] direction.

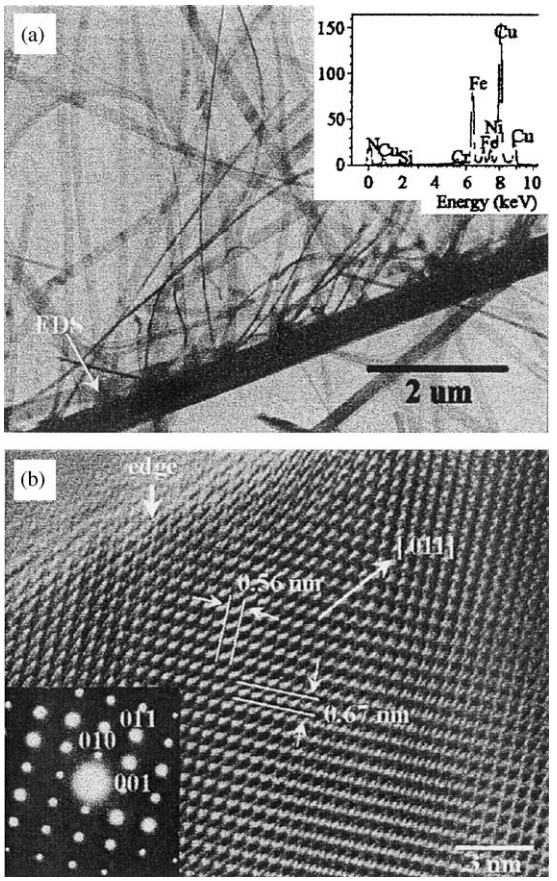

Fig. 5. (a) The typical TEM image of feather-like nanodendrites with EDS (inset) shows the spot consists of Fe, Ni, Cr and Si; the catalyst droplets are indicated by the arrow. (b) HRTEM image and SAED (inset) of the branch indicates that the branch grows along [0 1 1] direction.

there is no detectable Al. A possible explanation is the evaporation of the Al. The presence of the catalyst spots at the ends of the branches suggests liquid-based growth mechanisms. The spots are arranged with a regular distance along the middle line of the stem. There are no spots/branches observed anywhere else. Typically, more than one branch grow from each spot. EDS analysis on both stem and branches shows that they contain Si and N only with atomic ratio close to that for Si_3N_4. SAED analysis shows that the stem grows along [0 1 1]. Fig. 5b is a typical HRTEM of the branches. The images revealed that the branch possesses a perfect crystal structure with a few defects. The lattice fringe spacings of 0.56 and 0.67 nm correspond to (0 0 1) and (0 1 0) planes of α-Si_3N_4. The HRTEM and SAED (inset) indicate that the branches grew along [0 1 1] direction, which is the only growth direction for the branches.

No nanobelts and dendrites were observed for the samples without Al additives, suggesting the catalytic growth of the Si_3N_4 nanobelts in this study.

In the presence of a catalyst, nanostructures typically grow via the VLS mechanism [23], which is characterized by the presence of a catalyst droplet at the tips of the grown nanostructures [22] and requires a continuous supplement of Si/N-containing gaseous species. Previous study [21] on the pyrolysis of Ceraset without a catalyst revealed that the polysilazane was converted to an amorphous ceramic with an apparent composition of $SiC_{0.99}N_{0.84}$ at $\sim$1000 °C at 0.1 MPa N_2. This material was stable up to $\sim$1450 °C where it crystallized to Si_3N_4 and free carbon [24]. It can be seen that at present heat-treatment conditions (1300 °C, 0.1 MPa N_2), there is no Si-containing gaseous phase. That, together with the fact of the absence of a catalyst droplet at the tips of the nanobelts (Fig. 1b), suggests that the growth of nanostructures reported here is not via the VLS mechanism. We proposed a growth mechanism based on a solid–liquid–gas–solid (SLGS) reaction for the nanobelts. At the beginning of the process, the amorphous SiCN reacted with Al to form a liquid Si–Al–C alloy at a temperature higher than the eutectic temperature of Si–Al–C ternary system, meanwhile released N_2 gas. Further reaction of the solid SiCN and the liquid alloy resulted in a liquid supersaturated with silicon. This supersaturated liquid phase then reacted with N_2 gas to precipitate the Si_3N_4 nanobelts. The formation of silicon nitride, instead of silicon or silicon carbide, is due to the fact that the silicon nitride is the most stable phase at the processing conditions. However, the mechanism that governed the formation of nanobelts rather than nanowires is not clear.

Similarly, a two-stage SLGS growth mechanism is proposed for the growth of the nanodendrites.

First, Si_3N_4 plate-like stems were formed via the SLGS mechanism. The formation of relatively large-scale plate-like stems suggests the existence of large particles in the catalyst. The impurity elements such as Fe, Ni and Cr were then deposited onto the surfaces of the stem uniformly. Another possible source for the impurity elements is the amorphous layer that generally formed on the surface of liquid–solid grown structures [25]. Such impurities were then reacted with Si_3N_4 stem to nucleate liquid spots consisting of Si, Fe, Ni and Cr. Further reaction of the spots and the stem resulted in Si-supersaturated liquid. The nanobelt branches then nucleated and grew via reaction of N_2 gas and the supersaturated liquid at the surfaces of the liquid droplets. The uniform distribution of the impurities and subsequent nucleation are essential for the formation of catalyst spots with regular distribution. Investigations are required to further confirm the proposed growth mechanism.

4. Conclusion

In summary, Si_3N_4 nanobelts and nanodendrites were synthesized simultaneously via a novel catalyst-assisted crystallization of amorphous silicon carbonitride derived by the pyrolysis of polymeric precursor. The single-crystalline nanobelts, which grew along either [0 1 1] or [1 0 0] direction, have the thickness and width ranging from 20–30 nm and 100–200 nm, respectively, and up to several millimeters in length. The nanodendrites consist of a plate-like stem and nanobelts branches of 10–20 nm thick, 50–150 nm wide and up to 50 μm in length. The branches, which grew along [0 1 1] direction, grew only along the middle line of the stem with regular spacing. The growth mechanism for both nanobelts and nanodendrite is attributed to a solid–liquid–gas–solid process.

References

[1] G. Ziegler, J. Heinrich, C. Wötting, J. Mater. Sci. 22 (1987) 3041.
[2] R.K. Govila, J. Mater. Sci. 20 (1985) 4345.
[3] F. Munakata, K. Matsuo, K. Furuya, Y. Akimune, J. Ye, I. Ishikawa, Appl. Phys. Lett. 74 (1999) 3498.
[4] A.R. Zanatta, L.A.O. Nunes, Appl. Phys. Lett. 72 (1998) 3127.
[5] F. Giorgis, C.F. Pirri, C. Vinegoni, L. Pavesi, Phys. Rev. B 60 (1999) 572.
[6] S.V. Geshpande, E. Gulari, S.W. Brown, S.C. Rand, J. Appl. Phys. 77 (1998) 6534.
[7] Y. Zhang, N. Wang, R. He, Q. Zhang, J. Zhu, Y. Yan, J. Mater. Res. 15 (2000) 1048.
[8] X. Wu, W. Song, B. Zhao, W. Huang, M. Pu, Y. Sun, J. Du, Solid State Commun. 115 (2000) 683.
[9] Y. Zhang, N. Wang, R. He, J. Liu, X. Zhang, J. Zhu, J. Crystal Growth 233 (2001) 803.
[10] H. Kim, J. Park, H. Yang, Chem. Phys. Lett. 372 (2003) 269.
[11] L. Yin, Y. Bando, Y. Zhu, Y. Li, Appl. Phys. Lett. 83 (2003) 3584.
[12] W. Yang, H. Miao, Z. Xie, L. Zhang, L. An, Chem. Phys. Lett. 383 (1–2) (2004) 441.
[13] L. Cao, K. Hahn, Y. Wang, C. Scheu, Z. Zhang, C. Gao, Y. Li, X. Zhang, L. Sun, W. Wang, M. Rühle, Adv. Mater. 14 (2002) 1294.
[14] R. Ma, Y. Bando, T. Sato, L. Bourgeois, Diam. Relat. Mater. 11 (2002) 1397.
[15] J. Jian, X. Chen, W. Wang, L. Dai, Y. Xu, Appl. Phys. A 76 (2003) 291.
[16] Y. Zhu, W. Hu, W. Hsu, M. Terrones, N. Grobert, J.P. Hare, H.W. Kroto, D.R.M. Walton, H. Terrones, Chem. Phys. Lett. 309 (1999) 327.
[17] D. Kuang, A. Xu, Y. Fang, H. Liu, C. Frommen, D. Fenske, Adv. Mater. 15 (2003) 1747.
[18] M. Mo, Z. Zhu, X. Yang, X. Liu, S. Zhang, J. Gao, Y. Qian, J. Crystal Growth 256 (2003) 377.
[19] D. Chen, G. Shen, K. Tang, X. Jiang, L. Huang, Y. Jin, Y. Qian, Inorg. Chem. Commun. 6 (2003) 710.
[20] Z. Wang, X. Kong, J. Zuo, Phys. Rev. Lett. 91 (2003) 185502.
[21] Y. Xia, P. Yang, Y. Sun, Y. Wu, B. Mayers, B. Gates, Y. Yin, F. Kim, H. Yan, Adv. Mater. 15 (2003) 353.
[22] R.S. Wagner, W.C. Ellis, Appl. Phys. Lett. 4 (1964) 89.
[23] Y. Li, E. Kroke, R. Riedel, C. Fasel, C. Gervais, F. Babonneau, Appl. Organometal. Chem. 15 (2001) 820.
[24] H.J. Seifert, J. Peng, H.L. Lucas, F. Aldinger, J. Alloys Compounds 320 (2001) 251.
[25] T. Seeger, P. Kohler-Redlich, M. Rühle, Adv. Mater. 12 (2000) 279.